











Lifetime measurements of excited states in ^{57}Mn

H. Kleis , K. Arnsward , A. Blazhev , M. Droste , P. Reiter ,* R. Abels, R. Burggraf , A. Esmaylzadeh ,
C. Fransen , R. Hirsch , V. Karayonchev,[†] D. Luyken , J. Wehlitz, and D. Werner
Institut für Kernphysik, Universität zu Köln, D-50937 Köln, Germany



(Received 5 July 2023; accepted 9 November 2023; published 12 December 2023)

Excited states in ^{57}Mn are populated using the $^{55}\text{Mn}(^{18}\text{O}, ^{16}\text{O})^{57}\text{Mn}$ two-neutron transfer reaction at the FN tandem accelerator in Cologne. Lifetimes of excited nuclear states in ^{57}Mn were determined utilizing the Doppler-shift attenuation method. A comparison between experiment and shell-model theory was made for excitation energies and reduced transition strengths along the odd- Z isotopes Sc, V, Mn, and Co. The new results on transition strengths in ^{57}Mn are described well by the standard interactions GXPF1A and KB3G. The development along the $N = 32$ isotones for these odd- Z nuclei and discrepancies between experiment and theory are discussed.

DOI: [10.1103/PhysRevC.108.064308](https://doi.org/10.1103/PhysRevC.108.064308)

I. INTRODUCTION

Shell evolution in the neutron-rich isotopes from Ca to Ni is the subject of on-going research in theoretical and experimental nuclear physics. In particular, a detailed study of the two subshell closures at $N = 32$ and $N = 34$ is important in order to benchmark the shell-driving mechanisms away from stability. Experimentally, the subject is pursued by mass measurements and by spectroscopic studies of the exotic nuclei along isotopic chains.

Recent high-precision mass measurements of neutron-rich Ca, Ti, and V isotopes were performed at TRIUMF's Ion Trap for Atomic and Nuclear Science (TITAN) and the Low Energy Beam and Ion Trap (LEBIT) facilities [1]. At RIKEN the atomic masses of ^{55}Sc , $^{56,58}\text{Ti}$, and $^{56-59}\text{V}$ have been determined using the high-precision multireflection time-of-flight technique [2]. The TRIUMF measurements around $N = 32$ and $N = 34$ support the disappearance of the $N = 32$ shell closure with an increasing proton number above Ca; the new results do not support the presence of a shell closure at $N = 34$ for nuclei with an even-proton number higher than that of Ca. The RIKEN results confirm the nonexistence of the $N = 34$ two-neutron shell gaps for Ti and V.

However, signatures of subshell closures were also deduced from the excitation energy of the first 2^+ states in even-even nuclei, while more refined studies focus on the transition probabilities. For the Ca isotopes, the $N = 32$ and $N = 34$ subshell closures were deduced from the increased excitation energy of the first 2^+ states [3–5]. In addition, the energy of the first excited 2^+ state in the Ti and Cr isotopes increases at the neutron number $N = 32$ [6,7]. The subshell closure at $N = 32$ was also corroborated by a minimum in the

transition probabilities $B(E2; 2^+ \rightarrow 0^+)$ that were determined from lifetime measurements [8–10].

Shell-model interactions like GXPF1A and KB3G predicted these increased excitation energies of the first 2^+ state in the even-even nuclei at $N = 32$ by explaining it with a larger gap between the $\nu(p_{3/2})$ and $\nu(p_{1/2})$ orbitals. The size of this $N = 32$ shell gap decreases at higher proton numbers and vanishes completely in the iron isotopes with the proton number $Z = 26$ [5]. This is caused by the interplay between the proton and neutron orbitals as additional protons in the $\pi(f_{7/2})$ orbital reduce the single-particle energy of the neutron $\nu(f_{5/2})$ orbital so that the shell gap between the $\nu(p_{3/2})$ and $\nu(p_{1/2})$ orbital disappears.

For the discussion of a neutron subshell closure in the $Z = 25$, $N = 32$ isotope ^{57}Mn , the excitation energies of the $11/2^-$ and $9/2^-$ states and transition probabilities are considered. Previously ^{57}Mn was populated via fusion-evaporation reaction, transfer reaction, and β^- decay [11]. Lifetimes of excited states in ^{57}Mn were measured only by Nathan *et al.* via the $^{48}\text{Ca}(^{13}\text{C}, p3n)^{57}\text{Mn}$ fusion-evaporation reaction using the Doppler-Shift attenuation method (DSAM) [12]. No lifetime information of the $9/2^-$ state is known, while a lower limit for the lifetime of the $11/2^-$ state was determined to be $\tau(11/2^-) > 0.5$ ps [12]. In 2010, Steppenbeck *et al.* [13] measured angular distributions and expanded the level scheme up to spins of $25/2$ with an excitation energy of around 8 MeV after the $^{13}\text{C}(^{48}\text{Ca}, p3n)^{57}\text{Mn}$ fusion-evaporation.

The new measurement was motivated by the missing lifetime information in ^{57}Mn , which extends studies at $N = 32$ along Z , as well as the N (even) systematics for the Mn ($Z = 25$) isotopes. The paper is organized as follows. The experimental setup and its details are the subject of Sec. II. Details of the data analysis and new results are described in Sec. III. The discussion of shell-model results for odd-even nuclei in this region is the subject of Sec. IV.

*Corresponding author: preiter@ikp.uni-koeln.de

[†]Current address: Argonne National Laboratory, Argonne, IL 60439, USA.

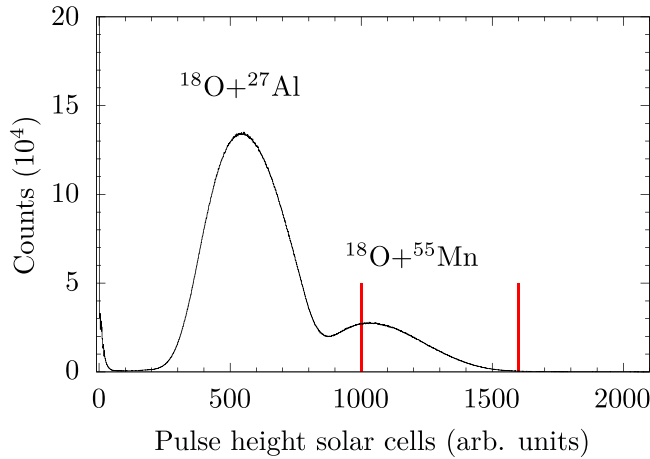


FIG. 1. Particle-energy spectrum of the solar cells is shown with two dominant peaks coming from reactions with the Al backing and the Mn target. The chosen gate for the γ -particle coincidence analysis is indicated in red.

II. EXPERIMENT

Lifetimes of excited states in the odd-even ^{57}Mn nucleus were determined using the DSAM. The experiment was performed at the FN tandem accelerator at the Institute for Nuclear Physics, University of Cologne, employing the $^{55}\text{Mn}(^{18}\text{O}, ^{16}\text{O})^{57}\text{Mn}$ two-neutron transfer reaction at 38-MeV beam energy. A setup of 11 high-purity germanium (HPGe) detectors was employed, positioned in two rings at polar angles of $\theta_1 = 45^\circ$ (six detectors) and $\theta_2 = 142.3^\circ$ (five detectors) with respect to the beam axis. To detect back-scattered beamlike oxygen ions after two-neutron transfer reactions in coincidence with γ -ray events, the setup was extended by six solar-cell particle detectors in the backward direction [14]. As the level lifetimes of interest are expected to be in the lower picosecond and sub-picosecond region, a DSAM foil was used consisting of a 0.4-mg/cm^2 ^{55}Mn target evaporated on a 3.5-mg/cm^2 ^{27}Al backing. Coincident γ -ray events were processed and recorded utilizing the NuDAQ data-acquisition system [15] employing 100-MHz synchronized V1782 and VX1730 digitizers as well as a V2495 logic module manufactured by CAEN S.p.A. The data were finally sorted into γ -particle coincidence matrices and were analyzed for the HPGe-detector rings under forward and backward angles separately. In total, 10^8 coincident γ -particle events were recorded and stored to disk.

In Fig. 1 the measured energy spectrum of the back-scattered ions in the solar cells is displayed. The lower-energy peak is caused by reactions of the ^{18}O beam with the ^{27}Al backing material. A separation between the different $^{16,17,18}\text{O}$ isotopes relating to the two-neutron transfer, the one-neutron transfer, and the inelastic scattering is not achieved due to the low angular granularity of the solar cells and the energy and angular straggling of the recoiling nuclei. The interesting γ rays from transfer reactions are enriched by gating on the marked region in Fig. 1.

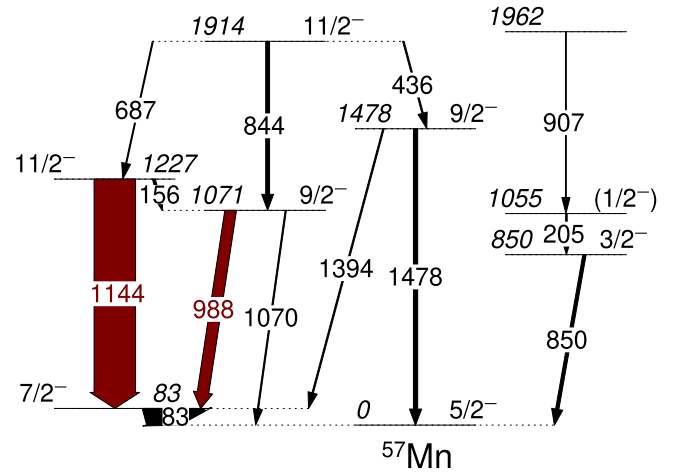


FIG. 2. Partial level scheme of populated excited states in ^{57}Mn . The widths of the shown arrows correspond to the intensity of the transition adopted from Ref. [13]. Excitation energies and transition energies are given in keV. The analyzed transitions are marked in red.

III. DATA ANALYSIS AND RESULTS

A partial level scheme of ^{57}Mn is given in Fig. 2. Excited states populated in this two-neutron transfer reaction are shown. Spins, parities, excitation energies, and transition energies are adopted from Ref. [13]. The thickness of the arrows is correlated to the intensity of the transition with respect to the $7/2^- \rightarrow 5/2_1^-$ transition with 100%, extracted from Ref. [13]. The lifetimes of the first $11/2_1^-$ and $9/2_1^-$ states were determined using their depopulating $11/2_1^- \rightarrow 7/2_1^-$ and $9/2_1^- \rightarrow 7/2_1^-$ transitions (marked in red).

The lifetimes are expected to be in the sub-picosecond regime. Therefore, the DSAM was exploited employing the APCAD program [16]. The stopping of the populated nuclei in the target and backing materials is calculated using Monte Carlo simulations. The electronic and nuclear stopping powers for each layer of the target are obtained from stopping and range of ions in matter (SRIM) [17]. Additionally, the utilized differential cross sections for the two-neutron-transfer reaction are calculated employing the GRAZING code [18,19]. Subsequently to the simulation of the two reaction partners, the γ -ray spectra are calculated for the different HPGe-detector angles. Simulated Doppler-broadened line shapes are fitted to the experimental spectra in order to extract the lifetimes. The final result is the weighted mean of lifetimes deduced for the two different HPGe-detector rings (see Figs. 3 and 4). The electronic and nuclear stopping powers, detector setup, and feeding are included with their uncertainties in the lifetime determination. The following experimental uncertainties are taken into account: electronic stopping, $\pm 6\%$ [20]; nuclear stopping, $\pm 10\%$ [21]; target thickness, $\pm 10\%$; and target rotation, $\pm 5^\circ$ [21]; angle of the HPGe detectors, $\pm 3^\circ$ [10]; distance of the HPGe to the target, ± 0.5 cm; distance to the solar cells, ± 0.3 cm, and size of the HPGe detectors, ± 0.1 cm [21]. For each uncertainty the effect on the lifetime is taken into account. The systematic errors of the lifetime associated with the uncertainties of the electronic and nuclear stopping powers are added in

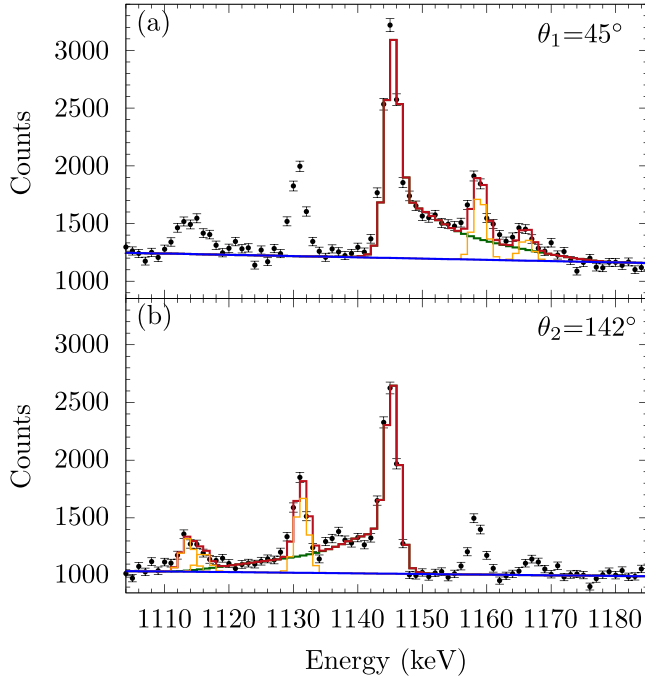


FIG. 3. γ -ray energy spectra for (a) forward and (b) backward angles are shown for the $11/2_1^- \rightarrow 7/2_1^-$ transition at 1144 keV. Spectra are produced by a gate on the two-neutron-transfer part in the particle spectrum. The final fit of the Doppler-broadened line shape is given in green. Additional contaminants are marked in orange and the background is given in blue lines. The convolution of all line-shape contributions is shown in red. See text for details.

quadrature and summed with the remaining systematic uncertainties stemming from the detector setup and feeding.

The γ -ray spectra and simulated line shapes (in red) are shown in Fig. 3 for the $11/2_1^- \rightarrow 7/2_1^-$ transition and in Fig. 4 for the $9/2_1^- \rightarrow 7/2_1^-$ transition, respectively, for the detector ring at (a) 45° and (b) 142° . The contaminants corresponding to transitions from various reactions with the ^{27}Al backing are marked in orange. For the lifetime analysis of the $9/2_1^-$ state, a contaminant is observed at a γ energy of 1015 keV. This transition results from an excited state in ^{27}Al populated via the inelastic scattering of the ^{18}O nuclei with the backing material and is included in the fit process. The lifetime of $\tau = 2.29(14)$ ps [22] of this transition in ^{27}Al is known and used to determine the contribution of the Doppler-shifted component to the line shape of the $9/2_1^- \rightarrow 7/2_1^-$ transition in ^{57}Mn for backward angles (142°). For the analysis of the lifetime at forward angles only the stopped component of this contaminant is considered within the fit region of the line shape of interest. Sharp lines of γ rays from completely stopped nuclei are visible in the fit region (orange marked peaks in Figs. 3 and 4). These transitions stem from excited nuclei populated in the fusion-evaporation reaction of the ^{18}O beam impinging on the ^{27}Al backing, e.g., ^{42}Ca and ^{39}K .

The long-lived ($\tau > 20$ ps) $11/2_2^-$ state is feeding into the $9/2_1^-$ state; this effect is taken into account for the lifetime analysis of the $9/2_1^-$ state. The slow-feeding components in

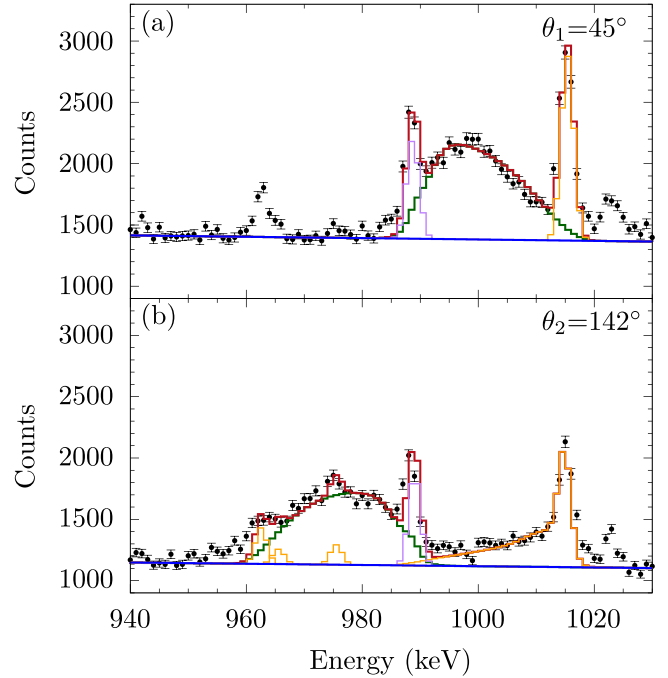


FIG. 4. γ -ray energy spectra for (a) forward and (b) backward angles are shown for the $9/2_1^- \rightarrow 7/2_1^-$ transition at 988 keV. The color code is similar to that of Fig. 3. Observed feeding contributions are given in purple.

the $9/2_1^-$ state produce a nonshifted peak, which is shown in Fig. 4 as a purple line. The $11/2_2^-$ state decays predominantly into the $9/2_1^-$ state, with a branching of 56(2)% and with a smaller fraction of 15(1)% into the $11/2_1^-$ state [13]. The feeding component resulting from the $11/2_2^- \rightarrow 11/2_1^-$ transition is considered in the error analysis. The final lifetime of the $9/2_1^-$ state yields $\tau = 0.60(^{+9}_{-8})$ ps. This lifetime corresponds to the reduced transition probability of $B(E2; 9/2_1^- \rightarrow 5/2_1^-) = 7.0(^{+13}_{-11})$ W.u.

The lifetime analysis of the $11/2_1^-$ state results in $\tau = 2.74(^{+18}_{-31})$ ps. The corresponding $B(E2; 11/2_1^- \rightarrow 7/2_1^-) = 10.9(^{+14}_{-7})$ W.u. is consistent with the previous upper limit of $B(E2; 11/2_1^- \rightarrow 7/2_1^-) < 60$ W.u. evaluated by Nathan *et al.* [12]. Both $9/2_1^-$ and $11/2_1^-$ states also decay via a mixed $M1/E2$ transition to the lower-lying $J - 1$ state. The corresponding $B(M1)$ values are calculated using the mixing ratios $\delta = 0.3(1)$ and $\delta = 0.15(5)$ correspondingly for the $9/2_1^- \rightarrow 7/2_1^-$ transition and the $11/2_1^- \rightarrow 9/2_1^-$ transition. These mixing ratios are determined from the attenuation coefficients assuming complete alignment [23] using the values $a_2 = 0.27(2)$ and $a_2 = -0.09(2)$ resulting from angular distribution measurements reported by Steppenbeck *et al.* [13]. For the $11/2_1^- \rightarrow 9/2_1^-$ transition the mixing ratio results in a large $B(E2)$ value that exceeds the recommended upper limit of 300 W.u. by 13%. The impact on the transition probabilities $B(M1; 11/2_1^- \rightarrow 9/2_1^-)$ and $B(E2; 11/2_1^- \rightarrow 7/2_1^-)$ is marginal within the uncertainties. The transition probabilities are summarized in Table I for the stretched $E2$ and the $M1$ component of the mixed $J \rightarrow J - 1$ transitions.

TABLE I. Experimental excitation energies from previous experimental values taken from Refs. [13], reduced transition strengths in W.u. of ^{57}Mn from the present experiment, and the results from GXPF1A and KB3G shell-model calculations are given. The γ intensities from Ref. [13] are used to deduce the transition probabilities. See text for details.

$J_i^\pi \xrightarrow{\sigma\lambda} J_f^\pi$	E_i (keV)			$B[\sigma\lambda; J_i^\pi \rightarrow (J - \lambda)_f^\pi]$		
	Expt.	GXPF1A	KB3G	Expt.	GXPF1A	KB3G
$9/2_1^- \xrightarrow{E2} 5/2_1^-$	1070 ^a	1206	1189	$7.0_{(-11)}^{(+13)}$	7.3	6.6
$9/2_1^- \xrightarrow{M1} 7/2_1^-$				$0.045_{(-6)}^{(+8)\text{b}}$	0.035	0.055
$11/2_1^- \xrightarrow{E2} 7/2_1^-$	1227 ^a	1296	1305	$10.9_{(-7)}^{(+14)}$	14.0	13.5
$11/2_1^- \xrightarrow{M1} 9/2_1^-$				$0.19_{(-2)}^{(+3)\text{c}}$	0.15	0.19

^aFrom Ref. [13].

^bDeduced using the experimental mixing ratio of $\delta = 0.3(1)$.

^cDeduced using the experimental mixing ratio of $\delta = 0.15(5)$.

IV. DISCUSSION

For the theoretical description of the excitation energies and reduced transition strengths, shell-model calculations were performed using the KSHELL code [24]. The $0f1p$ model space is used comprising the $0f_{7/2}$, $1p_{3/2}$, $1p_{1/2}$, and $0f_{5/2}$ proton and neutron orbitals coupled to a ^{40}Ca inert core. The calculations are based on the GXPF1A [25] and KB3G [26] interactions and utilize the effective charges $e_\pi = 1.31e$ and $e_\nu = 0.46e$ for protons and neutrons, respectively, as microscopically derived in Ref. [27]. In addition, the free g_s factors with a quenching of 0.9 are used in conjunction with the orbital g factors $g_{l,\pi} = 1.1$ and $g_{l,\nu} = -0.1$ [28].

In Figs. 5(a) and 6(a) excitation energies along the Mn line of isotopes for $N = 26$ – 36 are displayed for the first excited $9/2_1^-$ and $11/2_1^-$ states, respectively. The experimental excitation energies of the $9/2_1^-$ state show a maximum at the magic number $N = 28$. At higher neutron numbers $N > 28$ lower energies of comparable value are found. These energies are in good agreement with the results from the GXPF1A interaction within a maximum difference of 19% or a deviation on average of 107 keV. The KB3G interaction also reproduces the trend of the $E_{9/2_1^-}$ within a higher maximum difference of 23% and a deviation in average of 167 keV. It is noteworthy that the KB3G calculation yields a slightly increased $E_{9/2_1^-}$ energy at $N = 34$, unlike the GXPF1A interaction, and is different from experiment. In contrast to the $9/2_1^-$ states with a maximum at $N = 28$, the experimental energies of the $11/2_1^-$ states continuously decrease as a function of the neutron number. Both interactions describe the excitation energies of the $11/2_1^-$ states well, with the GXPF1A interaction being superior from $N = 28$ to 34.

In even-even nuclei the excitation energy and the reduced transition probability of the first excited 2^+ state are considered to be good signatures for the description of subshell closures. Evidence for shell closures can also be expected in odd-even systems like the Mn isotopes as the excited state of a single proton coupled to a neutron 2^+ state has comparable properties (i.e., large excitation energy, small $E2$ strength with respect to the ground state). Along the chain of Mn isotopes

the ground-state spin is predominantly $5/2_1^-$ apart from $7/2_1^-$ at $^{53}\text{Mn}_{28}$. Thus, the state with dominant single-proton configuration coupled to a neutron 2^+ configuration would be the $11/2_1^-$ state for $^{53}\text{Mn}_{28}$, while for the other Mn isotopes above $N = 28$ one expects this to be the $9/2_1^-$ state.

The $E2$ strengths are given in Figs. 5(b) and 6(b) for the $9/2_1^- \rightarrow 5/2_1^-$ and $11/2_1^- \rightarrow 7/2_1^-$ transitions, respectively. The literature experimental $B(E2)$ values (black triangles) are adopted from Ref. [11] complemented by values in $^{59,61}\text{Mn}$ (gray squares) obtained from Ref. [29]. Along the Mn isotope chain the experimental $B(E2; 9/2_1^- \rightarrow 5/2_1^-)$ values show minima at $N = 28$ and $N = 34$ [see Fig. 5(b)]. While both shell-model interactions match the minimum at $N = 28$, the minimum at $^{59}\text{Mn}_{34}$ is not reproduced. Apart from $N = 34$, both calculations show good agreement with the experimental values. The KB3G and GXPF1A interactions reproduce the $B(E2)$ values of the $11/2_1^- \rightarrow 7/2_1^-$ transitions well with a slight underestimation for $N \leq 30$ [see Fig. 6(b)].

The $B(M1)$ values for the $9/2_1^- \rightarrow 7/2_1^-$ transition are presented in Fig. 5(c). The experimental $B(M1)$ values for these transitions in the $^{59,61}\text{Mn}$ isotopes ($N = 34$ and 36) could not be deduced from the known lifetime values due to unknown mixing ratios. The known $B(M1)$ values from $N = 26$ to 32 vary along the isotopes, but show a minimal value of $B(M1; 9/2_1^- \rightarrow 7/2_1^-) = 0.0012(3)$ W.u. at $N = 28$. The shown Mn experimental $B(M1)$ values are reproduced well by these shell-model interactions. In contrast to this, there are still some discrepancies in that region between experimental $M1$ strengths and SM results. The KB3G and GXPF1A interactions predict in $^{53}\text{Ti}_{28}$ for the $5/2_1^- \rightarrow 3/2_1^-$ transition a spin-flip type $\nu(p_{3/2}) \leftrightarrow (p_{1/2})$ character and overestimate the $B(M1)$ value by nearly a factor of 4 [30]. Furthermore, both interactions include a too weak neutron core excitation and underestimate the $B(M1; 5/2_1^- \rightarrow 3/2_1^-)$ in ^{55}Cr [10].

The new $M1$ and $E2$ strengths in ^{57}Mn extend the known experimental results to higher neutron numbers. Both are in very good agreement with the shell-model interactions.

To discuss the subshell closure at $N = 32$ as a function of Z (odd) we focus on excitation energies and $B(E2)$ values for

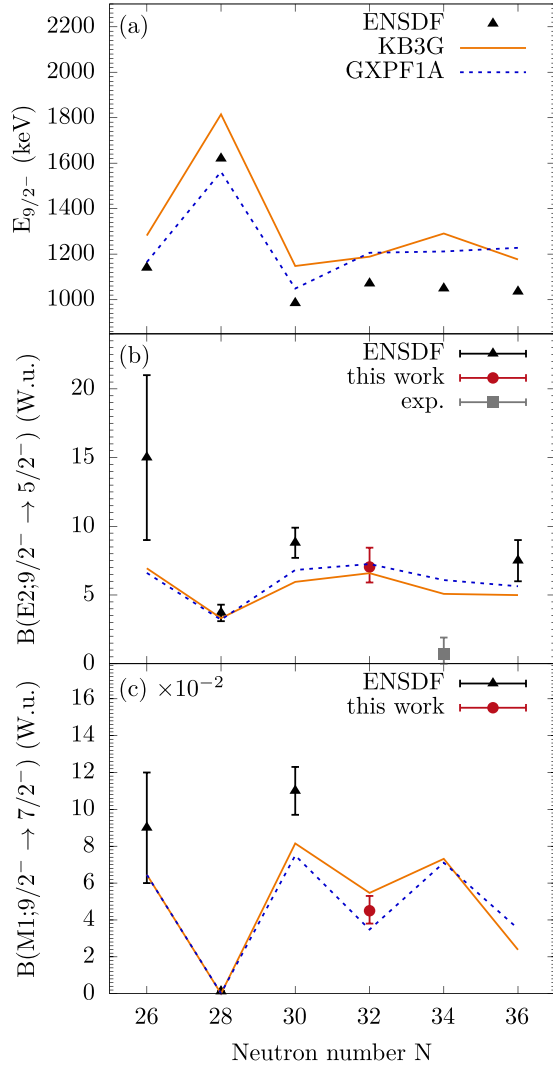


FIG. 5. Comparison between experimental and shell-model values for the odd-even Mn isotopes with neutron numbers $N = 26$ – 36 : (a) excitation energies $E_{9/2^-}$ of the $9/2^-$ state, (b) $B(E2; 9/2^- \rightarrow 5/2^-)$ values, and (c) $B(M1; 9/2^- \rightarrow 7/2^-)$ values. Adopted values (black triangles) from Ref. [11], the new results (red dots), and additional results (gray squares) obtained from Braunroth [29] are compared with the results of GXPF1A (blue dashed line) and KB3G (solid orange line) shell-model interactions.

the $9/2^-$ and $11/2^-$ states and the corresponding $J \rightarrow J - 2$ transitions along the Sc, V, Mn, and Co isotopes. As presented above, results along the Mn chain are described by KB3G and GXPF1A interactions. Similar results with respect to the KB3G and GXPF1A interactions were presented in Ref. [10] for excitation energies and transition strengths along $N = 31$ from Ti to Zn. The GXPF1A interaction is in most cases able to reproduce the experimental findings better than the KB3G interaction. Therefore, the comparison between SM results and experimental values in Figs. 7 and 8 are given for the GXPF1A interaction. In general, GXPF1A reproduces the energies of the states in the considered nuclei remarkably well up to $N = 34$. For heavier isotopes of $N > 34$, minor discrepancies are visible and it would be adequate to exchange

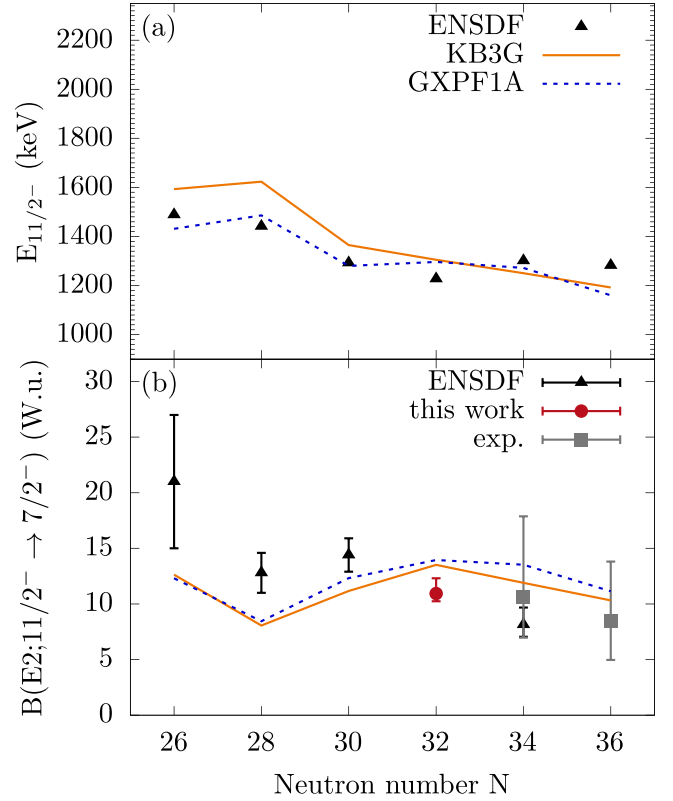


FIG. 6. Comparison between experimental and shell-model values for the odd-even Mn isotopes with neutron numbers $N = 26$ – 36 . (a) Excitation energies $E_{11/2^-}$ of the $11/2^-$ state and (b) $B(E2; 11/2^- \rightarrow 7/2^-)$ values. Same references and color code as in Fig. 5.

the interaction with the GXPF1Br interaction as in Ref. [5]. Generally, it would be of great interest to obtain the missing excitation energies for the $9/2^-$ and $11/2^-$ states in Sc and V for $N = 34$ and 36 .

The excitation energy of the $11/2^-$ state increases for the Sc, V, and Co isotopes at the magic neutron number $N = 28$; however, in the Mn isotopes the excitation energy shows a constant progression [see Fig. 8(a)]. Moreover, the energy of the $11/2^-$ state in the scandium and vanadium isotopes increases up to the neutron number $N = 32$ and decreases for higher neutron numbers. This corroborates the subshell closure at $N = 32$ for nuclei with proton numbers near calcium as it can be observed in the even-even Ti and Cr isotopes [6–9]. In contrast, the excitation energy of the Mn and Co isotopes shows a constant trend at higher neutron numbers. Adding more valence protons to the $\pi(f_{7/2})$ orbital reduces the energy of the $\nu(f_{5/2})$ orbital, and the local shell gap at $N = 32$ disappears as it is observed in the even-even Fe isotopes.

Another signature for shell and subshell closures is the $B(E2)$ value of the ground-state transition. In Fig. 7(b) the $B(E2; 9/2^- \rightarrow 5/2^-)$ values are shown for all odd(Z)-even(N) nuclei between Ca and Ni with neutron numbers $N = 26$ – 36 . Our new result completes the systematics for the Mn isotopes at $N = 32$; and it is perfectly reproduced by the GXPF1A shell model. Neither the experimental nor the

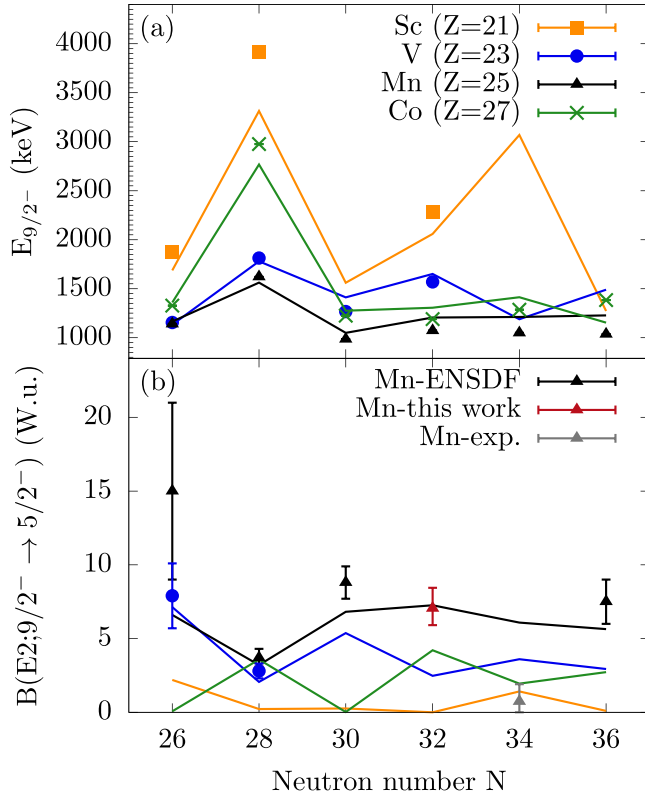


FIG. 7. (a) Calculated and experimental excitation energies $E_{9/2^-}$ in keV for the $9/2^-$ state and (b) $B(E2; 9/2^- \rightarrow 5/2^-)$ values in W.u. (from Refs. [11,29] and this work) for the odd-even Sc (squares), V (points), Mn (triangles), and Co (crosses) isotopes for neutron numbers $N = 26$ – 36 . The shell-model interaction GXPF1A (lines) is employed for the calculation.

theoretical excitation energies of the $9/2^-$ state are increased. The transition probability of the $9/2^- \rightarrow 5/2^-$ ground-state transition has a minimum at the $N = 32$ ^{57}Mn isotope, indicating clearly the vanishing of the $N = 32$ subshell closure at $Z = 25$.

On the other hand there is a discrepancy between the value for the $B(E2; 9/2^- \rightarrow 5/2^-)$ transition in ^{59}Mn [29] and the SM calculations. A possible explanation would be, for example, an inadequate model space of the GXPF1A interaction for this transition, neglecting the impact of higher-lying orbitals like $\nu g_{9/2}$ and $d_{5/2}$. On the other hand, large-scale shell-model calculations for the odd-even isotopes $^{51-63}\text{Mn}$ using the LNPS interaction in the extended proton- fp and neutron- $f5pg9d5$ model space have been reported [31]. It was found that the neutron $\nu g_{9/2}$ and $d_{5/2}$ orbitals are required in the model space in order to reproduce the magnetic moments of the ground state for ^{61}Mn and heavier isotopes. Also Monte Carlo shell-model calculations with the modified A3DA interaction in the extended proton-neutron $f5pg9d5$ model space [32] demonstrate that the effect of the higher-lying orbitals $\nu g_{9/2}$ and $d_{5/2}$ for Mn isotopes up to $N = 34$ can be considered negligible. Therefore, this discrepancy between theory and experiment for ^{59}Mn [29] needs further attention and possibly an independent experimental confirmation. Furthermore,

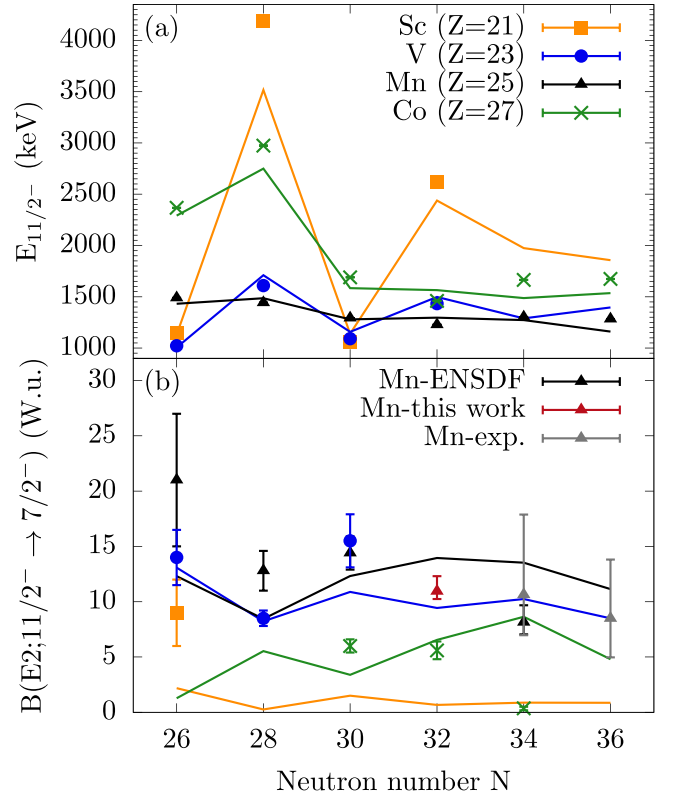


FIG. 8. (a) Calculated and experimental excitation energies $E_{11/2^-}$ in keV for the $11/2^-$ state and (b) $B(E2; 11/2^- \rightarrow 7/2^-)$ values in W.u. (from Refs. [11,29] and this work) for the odd-even Sc (squares), V (points), Mn (triangles), and Co (crosses) isotopes for neutron numbers $N = 26$ – 36 . The shell-model interaction GXPF1A is employed for the calculation.

Fig. 7(b) illustrates that with the exception of the complete Mn chain and two experimental points for vanadium isotopes, no other experimental values are known for the transition strength in these nuclei.

In Fig. 8(b) the $B(E2; 11/2^- \rightarrow 7/2^-)$ values are shown for all odd-even nuclei between Ca and Ni with neutron numbers $N = 26$ – 36 . For Sc, only one experimental $B(E2; 11/2^- \rightarrow 7/2^-)$ value is available at $N = 26$, which is underestimated by the GXPF1A interaction [see Fig. 8(b)]. In contrast to the Sc isotopes, the $E2$ transition probabilities are in very good agreement with the shell-model results along the V-isotope chain. In addition, the adopted $B(E2)$ values in the vanadium isotopes are minimal for $N = 28$ and also the $E2$ strength decreases at $N = 32$ as calculated with the GXPF1A interaction.

The shell-model results indicate a subshell closure at $N = 32$ in the $Z = 21$ and $Z = 23$ isotopes due to a decreased $B(E2; 11/2^- \rightarrow 7/2^-)$ value. For the Co isotopes one notes a small deviation for the $B(E2)$ value at $N = 30$ and a large drop of the experimental $E2$ strength at $N = 34$, which is not reproduced by the GXPF1A calculation. In this case the reason for the discrepancy may be related to the limited model space and the missing higher-lying neutron orbitals. The discrepancy between theory and experiment at ^{61}Co also needs future investigation, in particular, a new lifetime measurement.

The shell closures at $N = 28$ are reproduced by the smaller theoretical $E2$ strengths for the decay of $9/2_1^-$ and $11/2_1^-$ states in the Sc, V, and Mn isotopes. Theoretical results concur with the experimental decrease in $E2$ strength at $N = 28$ in these chains [see Figs. 7(b) and 8(b)]. In contrast, the predicted $B(E2)$ values for these transitions are enhanced relative to the neighboring Co isotopes at $N = 28$. This can be related to the vicinity of the $N = Z = 28$ “LS-open” ^{56}Ni core, where recent measurements have found increased $E2$ transition strengths for higher excited states $>2^+$ along the yrast line [33].

V. CONCLUSIONS

To summarize, new lifetimes for the $9/2_1^-$ and $11/2_1^-$ states in ^{57}Mn were determined. The experimentally deduced transition probabilities were compared along the Mn isotopic chain with two shell-model interactions, GXPF1A and KB3G, in the $0f1p$ model space with a filled ^{40}Ca core. Calculations of $B(E2)$ and $B(M1)$ transition strengths and excitation energies are generally in good agreement for the examined

Mn isotopes for the $9/2_1^-$ and $11/2_1^-$ states. These results support the observation that large-scale shell-model calculations with the employed interaction reflect the experimental results well. However, remaining open questions arise for ^{59}Mn and ^{61}Co where experimental values cannot be reproduced by the GXPF1A interaction. In both cases an extended shell-model space with the higher-lying neutron orbitals $\nu g_{9/2}$ and $d_{5/2}$ should be employed in future calculations. In addition, new lifetime measurements are not only needed in these two isotopes but also in many neighboring isotopes where the existing data base of $B(E2)$ values is still very sparse.

ACKNOWLEDGMENTS

We thank the IKP FN Tandem accelerator team for the tireless support during the experiment. We acknowledge funding by the Deutsche Forschungsgemeinschaft for the upgrade of the used high-purity germanium detectors under Grant No. INST 216/988-1 FUGG.

-
- [1] W. S. Porter, E. Dunling, E. Leistenschneider, J. Bergmann, G. Bollen, T. Dickel, K. A. Dietrich, A. Hamaker, Z. Hockenbery, C. Izzo, A. Jacobs, A. Javaji, B. Kootte, Y. Lan, I. Miskun, I. Mukul, T. Murböck, S. F. Paul, W. R. Plaß, D. Puentes *et al.*, Investigating nuclear structure near $N = 32$ and $N = 34$: Precision mass measurements of neutron-rich Ca, Ti, and V isotopes, *Phys. Rev. C* **106**, 024312 (2022).
- [2] S. Iimura, M. Rosenbusch, A. Takamine, Y. Tsunoda, M. Wada, S. Chen, D. S. Hou, W. Xian, H. Ishiyama, S. Yan, P. Schury, H. Crawford, P. Doornenbal, Y. Hirayama, Y. Ito, S. Kimura, T. Koiwai, T. M. Kojima, H. Koura, J. Lee *et al.*, Study of the $N = 32$ and $N = 34$ shell gap for Ti and V by the first high-precision multireflection time-of-flight mass measurements at BigRIPS-SLOWRI, *Phys. Rev. Lett.* **130**, 012501 (2023).
- [3] A. Huck, G. Klotz, A. Knipper, C. Miehé, C. Richard-Serre, G. Walter, A. Poves, H. L. Ravn, and G. Marguier, Beta decay of the new isotopes ^{52}K , ^{52}Ca , and ^{52}Sc ; a test of the shell model far from stability, *Phys. Rev. C* **31**, 2226 (1985).
- [4] A. Gade, R. V. F. Janssens, D. Bazin, R. Broda, B. A. Brown, C. M. Campbell, M. P. Carpenter, J. M. Cook, A. N. Deacon, D.-C. Dinca, B. Fornal, S. J. Freeman, T. Glasmacher, P. G. Hansen, B. P. Kay, P. F. Mantica, W. F. Mueller, J. R. Terry, J. A. Tostevin, and S. Zhu, Cross-shell excitation in two-proton knockout: Structure of ^{52}Ca , *Phys. Rev. C* **74**, 021302(R) (2006).
- [5] D. Steppenbeck, S. Takeuchi, N. Aoi, P. Doornenbal, M. Matsushita, H. Wang, H. Baba, N. Fukuda, S. Go, M. Honma, J. Lee, K. Matsui, S. Michimasa, T. Motobayashi, D. Nishimura, T. Otsuka, H. Sakurai, Y. Shiga, P.-A. Söderström, T. Sumikama *et al.*, Evidence for a new nuclear ‘magic number’ from the level structure of ^{54}Ca , *Nature (London)* **502**, 207 (2013).
- [6] R. V. F. Janssens, B. Fornal, P. F. Mantica, B. A. Brown, R. Broda, P. Bhattacharyya, M. P. Carpenter, M. Cinausero, P. J. Daly, A. D. Davies, T. Glasmacher, Z. W. Grabowski, D. E. Groh, M. Honma, F. G. Kondev, W. Królas, T. Lauritsen, S. N. Liddick, S. Lunardi, N. Marginean *et al.*, Structure of $^{52,54}\text{Ti}$ and shell closures in neutron-rich nuclei above ^{48}Ca , *Phys. Lett. B* **546**, 55 (2002).
- [7] R. Chapman, S. Hinds, and A. E. MacGregor, A study of ^{52}Cr , ^{54}Cr and ^{56}Cr by the (t, p) reaction, *Nucl. Phys. A* **119**, 305 (1968).
- [8] A. Goldkuhle, C. Fransen, A. Blazhev, M. Beckers, B. Birkenbach, T. Braunroth, E. Clément, A. Dewald, J. Dudouet, J. Eberth, H. Hess, B. Jacquot, J. Jolie, Y.-H. Kim, A. Lemasson, S. M. Lenzi, H. J. Li, J. Litzinger, C. Michelagnoli, C. Müller-Gatermann *et al.* (AGATA Collaboration), Lifetime measurements in $^{52,54}\text{Ti}$ to study shell evolution toward $N = 32$, *Phys. Rev. C* **100**, 054317 (2019).
- [9] M. Seidlitz, P. Reiter, A. Dewald, O. Möller, B. Bruyneel, S. Christen, F. Finke, C. Fransen, M. Górska, H. Grawe, A. Holler, G. Ilie, T. Kotthaus, P. Kudejová, S. M. Lenzi, S. Mandal, B. Melon, D. Mücher, J.-M. Regis, B. Saha *et al.*, Precision lifetime measurements of the first 2^+ and 4^+ states in ^{56}Cr at the $N = 32$ subshell closure, *Phys. Rev. C* **84**, 034318 (2011).
- [10] H. Kleis, M. Seidlitz, A. Blazhev, L. Kaya, P. Reiter, K. Arnsward, A. Dewald, M. Droste, C. Fransen, O. Möller, N. Shimizu, Y. Tsunoda, Y. Utsuno, P. von Brentano, and K. O. Zell, Lifetime measurements of excited states in ^{55}Cr , *Phys. Rev. C* **104**, 034310 (2021).
- [11] Evaluated Nuclear Structure Data File (ENSDF), 2020, <http://www.nndc.bnl.gov/ensdf>.
- [12] A. M. Nathan, J. W. Olness, E. K. Warburton, and J. B. McGrory, Yrast decay schemes from heavy-ion $+^{48}\text{Ca}$ fusion-evaporation reactions. III. $^{57,58}\text{Fe}$, $^{54,55}\text{Cr}$, and $^{57,58}\text{Mn}$, *Phys. Rev. C* **17**, 1008 (1978).
- [13] D. Steppenbeck, A. N. Deacon, S. J. Freeman, R. V. F. Janssens, S. Zhu, M. P. Carpenter, P. Chowdhury, M. Honma, T. Lauritsen, C. J. Lister, D. Seweryniak, J. F. Smith, S. L. Tabor, and B. J. Varley, High-spin structures in the neutron-rich isotopes $^{57-60}\text{Mn}$, *Phys. Rev. C* **81**, 014305 (2010).
- [14] M. Beckers, C. Müller-Gatermann, A. Blazhev, T. Braunroth, A. Dewald, C. Fransen, A. Goldkuhle, L. Kornweibel, J.

- Litzinger, F. von Spee, and K.-O. Zell, Lifetime measurement of excited states in ^{144}Ce : Enhanced $E1$ strengths in a candidate for octupole deformation, *Phys. Rev. C* **102**, 014324 (2020).
- [15] M. Weinert, Investigation of microscopic structures in the low-energy electric dipole response of ^{120}Sn using consistent experimental and theoretical observables and digital signal processing for nuclear physics experiments, Ph.D. thesis, Universität zu Köln, 2022, <https://kups.ub.uni-koeln.de/65390/>.
- [16] C. Stahl, J. Leske, M. Lettmann, and N. Pietralla, APCAD–Analysis program for the continuous-angle DSAM, *Comput. Phys. Commun.* **214**, 174 (2017).
- [17] J. F. Ziegler, M. D. Ziegler, and J. P. Biersack, SRIM–The stopping and range of ions in matter, *Nucl. Instrum. Methods Phys. Res., Sect. B* **268**, 1818 (2010).
- [18] R. Yanez and W. Loveland, Predicting the production of neutron-rich heavy nuclei in multinucleon transfer reactions using a semi-classical model including evaporation and fission competition, GRAZING-F, *Phys. Rev. C* **91**, 044608 (2015).
- [19] A. Winther, Grazing reactions in collisions between heavy nuclei, *Nucl. Phys. A* **572**, 191 (1994).
- [20] Interactions of Ions with matter–SRIM, 2020, <http://www.srim.org>.
- [21] V. Karayonchev, J. Jolie, A. Blazhev, A. Dewald, A. Esmaylzadeh, C. Fransen, G. Häfner, L. Knafla, J. Litzinger, C. Müller-Gatermann, J.-M. Régis, K. Schomacker, A. Vogt, N. Warr, A. Leviatan, and N. Gavrielov, Tests of collectivity in ^{98}Zr by absolute transition rates, *Phys. Rev. C* **102**, 064314 (2020).
- [22] P. Tikkanen, J. Keinonen, V. Karttunen, and A. Kuronen, Transition strengths in the mirror nuclei ^{27}Si – ^{27}Al , *Nucl. Phys. A* **456**, 337 (1986).
- [23] E. der Mateosian and A. W. Sunyar, Tables of angular-distribution coefficients for gamma rays of mixed multipolarities emitted by aligned nuclei, *At. Data Nucl. Data Tables* **13**, 407 (1974).
- [24] N. Shimizu, T. Mizusaki, Y. Utsuno, and Y. Tsunoda, Thick-restart block Lanczos method for large-scale shell-model calculations, *Comput. Phys. Commun.* **244**, 372 (2019).
- [25] M. Honma, T. Otsuka, B. A. Brown, and T. Mizusaki, Shell-model description of neutron-rich pf-shell nuclei with a new effective interaction GXPFI, *Eur. Phys. J. A* **25**, 499 (2005).
- [26] A. Poves, J. Sánchez-Solano, E. Caurier, and F. Nowacki, Shell model study of the isobaric chains $A = 50$, $A = 51$ and $A = 52$, *Nucl. Phys. A* **694**, 157 (2001).
- [27] M. Dufour and A. P. Zuker, Realistic collective nuclear Hamiltonian, *Phys. Rev. C* **54**, 1641 (1996).
- [28] M. Honma, T. Otsuka, B. A. Brown, and T. Mizusaki, New effective interaction for pf -shell nuclei and its implications for the stability of the $N = Z = 28$ closed core, *Phys. Rev. C* **69**, 034335 (2004).
- [29] T. Braunroth, Lifetime measurements in neutron-rich isotopes close to $N = 40$ and development of a simulation tool for RDDS spectra, Ph.D. thesis, Universität zu Köln, 2017, <https://kups.ub.uni-koeln.de/7956/>.
- [30] A. Goldkuhle, A. Blazhev, C. Fransen, A. Dewald, M. Beckers, B. Birkenbach, T. Braunroth, E. Clément, J. Dudouet, J. Eberth, H. Hess, B. Jacquot, J. Jolie, Y.-H. Kim, A. Lemasson, S. M. Lenzi, H. J. Li, J. Litzinger, C. Michelagnoli, C. Müller-Gatermann *et al.*, Lifetime measurements of excited states in neutron-rich ^{53}Ti : Benchmarking effective shell-model interactions, *Phys. Rev. C* **102**, 054334 (2020).
- [31] C. Babcock, H. Heylen, J. Billowes, M. L. Bissell, K. Blaum, P. Campbell, B. Cheal, R. F. Garcia Ruiz, C. Geppert, W. Gins, M. Kowalska, K. Kreim, S. M. Lenzi, I. D. Moore, R. Neugart, G. Neyens, W. Nörtershäuser, J. Papuga, and D. T. Yordanov, Evidence for increased neutron and proton excitations between $^{51-63}\text{Mn}$, *Phys. Lett. B* **750**, 176 (2015).
- [32] C. Babcock, H. Heylen, M. L. Bissell, K. Blaum, P. Campbell, B. Cheal, D. Fedorov, R. F. Garcia Ruiz, W. Geithner, W. Gins, T. Day Goodacre, L. K. Grob, M. Kowalska, S. M. Lenzi, B. Maass, S. Malbrunot-Ettenauer, B. Marsh, R. Neugart, G. Neyens, W. Nörtershäuser *et al.*, Quadrupole moments of odd- A $^{53-63}\text{Mn}$: Onset of collectivity towards $N = 40$, *Phys. Lett. B* **760**, 387 (2016).
- [33] K. Arnsward, A. Blazhev, F. Nowacki, P. Petkov, P. Reiter, T. Braunroth, A. Dewald, M. Droste, C. Fransen, R. Hirsch, V. Karayonchev, L. Kaya, L. Lewandowski, C. Müller-Gatermann, M. Seidlitz, B. Siebeck, A. Vogt, D. Werner, and K.O. Zell, Enhanced quadrupole collectivity in doubly-magic ^{56}Ni : Lifetime measurements of the 4_1^+ and 6_1^+ states, *Phys. Lett. B* **820**, 136592 (2021).